Volume 49, Issue 1, July 1, 2010
ISSN 0891-5849

ELSEVIER

FREE RADICAL BIOLOGY & MEDICINE

The Official Journal of the
Society for Free Radical
Biology and Medicine

An Affiliate Journal of
the International Society
for Free Radical Research

Founding Editors:
Kelvin J. A. Davies, William A. Pryor

25 Years

Original Contribution

Proteomics study of oxidative stress and Src kinase inhibition in H9C2 cardiomyocytes: a cell model of heart ischemia–reperfusion injury and treatment

Hsiu-Chuan Chou [a,1], Yi-Wen Chen [b,1], Tian-Ren Lee [b], Fen-Shiun Wu [b], Hsin-Tsu Chan [b], Ping-Chiang Lyu [b], John F. Timms [c], Hong-Lin Chan [b,*]

[a] Tissue Regeneration Bio-Device Tech Lab, Medical Electronics and Device Technology Center, Industrial Technology Research Institute, Hsinchu 31040, Taiwan
[b] Institute of Bioinformatics and Structural Biology, National Tsing Hua University, Hsinchu 30013, Taiwan
[c] Cancer Proteomics Laboratory, EGA Institute for Women's Health, University College London, London, UK

ARTICLE INFO

ABSTRACT

Protein phosphorylation plays a crucial role in the signal transduction pathways that regulate gene expression, metabolism, cell adhesion, and cell survival in response to oxidative stress. In this study, we have used hydrogen peroxide treatment of H9C2 rat cardiomyocytes as a model of oxidative stress in heart ischemia–reperfusion injury. We show that oxidative stress induces a robust tyrosine phosphorylation of multiple proteins in this cell type. A phosphoproteomics approach using anti-phosphotyrosine affinity purification and LC–MS/MS was then used to identify the protein targets of this stress-induced phosphorylation. Twenty-three tyrosine-phosphorylated proteins were identified, with the majority known to be associated with cell–cell junctions, the actin cytoskeleton, and cell adhesion. This suggested that oxidative stress may have a profound effect on intercellular connections and the cytoskeleton to affect cell adhesion, morphology, and survival. Importantly, Src kinase was shown to be a major upstream regulator of these events. Immunofluorescence studies, fluorescence-activated cell sorting, and cell-based assays were used to demonstrate oxidative stress-induced modification of cell adhesion structures and the cytoskeleton, induced de-adhesion, and increased apoptosis, which were reversed by treatment with the Src kinase inhibitor PP1. These data demonstrate the critical role of Src kinase in oxidative stress-induced phosphorylation and cell damage in cardiomyocytes and suggest that targeting this kinase may be an effective strategy for preventing ischemia–reperfusion injury in the heart.

© 2010 Elsevier Inc. All rights reserved.

Posttranslational modifications are the major regulators of protein activity, function, and localization. Protein phosphorylation in particular plays important roles in the regulation of signal transduction, gene expression, metabolism, and survival [1,2]. In mammalian cells, one-third of expressed proteins are thought to be phosphorylated at serine, threonine, and, less commonly (0.05–0.1%), tyrosine residues [3,4]. Although all types of phosphorylation are important for maintaining protein function and cell activities, tyrosine phosphorylation plays a crucial role in signal transduction that affects cell proliferation, mitogenesis, differentiation, cell death, and motility. Unregulated tyrosine phosphorylation may lead to diseases such as cancer by generating inappropriate proliferation and survival signals [5]. However, because of the low abundance of tyrosine-phosphorylated proteins, enrichment of these proteins is essential for studying the function of tyrosine phosphorylation. Currently, several strategies, such as immobilized metal-ion affinity chromatography [6,7], chemical modification [8], and affinity purification [9,10], have been used to enrich phosphoproteins. Among these strategies, antibody-based affinity purification can specifically and efficiently pull down tyrosine-phosphorylated proteins from cell lysates for protein analysis.

Reactive oxygen species (ROS)[2] comprise several species such as hydrogen peroxide (H_2O_2), the hydroxyl radical ($^\bullet OH$), superoxide ($O_2^{\bullet-}$), and singlet oxygen ($^\bullet O$). Their formation and related cytotoxicity have been described in previous reports [11–13]. ROS were originally recognized as products of the mammalian host defense mechanism, but have since been widely reported to play an important role in cell signaling and apoptosis. Among the ROS, H_2O_2 is the dominant form in cells, as it is more stable compared to the other ROS [14]. In addition, H_2O_2 has been reported to play an

important role in reversible protein phosphorylation in many cell signaling pathways via mediating the inactivation of protein tyrosine phosphatases (PTPs), PTEN, and peroxiredoxins by modification of their active-site cysteines to form Cys–OH or disulfide bonds. Thus, H_2O_2 has been recognized as a secondary messenger molecule in cells [15–19].

In cardiomyocytes, oxygen is reduced by two pathways: the dominant pathway is via the mitochondrial electron transport system, which reduces 95% of oxygen to H_2O; the remaining 5% of oxygen is processed by intracellular enzymes to produce ROS [20]. Although endogenous ROS seem to play important roles in regulating normal cellular processes and the intracellular antioxidant system can balance the effect of ROS under normoxic conditions, under certain pathological conditions, the antioxidant defense system is undermined and ROS-induced damage to the tissue can occur. Such injury occurs during ischemia–reperfusion, in which a shortage of blood supply to a region of the tissue for a certain period is followed by resumption of blood flow. The degree of the damage from ischemia–reperfusion depends on the duration and the extent of the hypoperfusion. In recent studies, cardiomyocyte damage induced by ischemia–reperfusion has been shown to be largely due to the generation of ROS [21–23]. However, the detailed mechanisms of ROS-induced cardiac tissue damage during myocardial ischemia–reperfusion injury are poorly understood. Some reports showed that ROS were able to damage the sarcoplasmic reticulum of the heart causing Ca^{2+} release and contractile dysfunction by modifying the structure and function of cardiac proteins [24,25]. This indicated that changes in the redox state of cardiac proteins play an important role in the early stage of myocardial ischemia and reperfusion injury.

In this study, we have identified and characterized the proteins that are phosphorylated in response to oxidative stress after treatment with H_2O_2 and relate these changes to the biological effects of oxidant treatment. The H9C2 rat cardiomyocyte cell line was chosen as a cellular model for these studies as this cell line retains the characteristics of isolated primary cardiomyocytes [26–30] and has been used as a model in ischemia and reperfusion studies [31]. Our work reveals that numerous cytoskeletal and adhesion-related proteins are targets of H_2O_2-induced phosphorylation in H9C2 cells and that the Src kinase is a critical upstream kinase regulating these events.

Materials and methods

Cell lines, cell culture, cell treatment

The rat cardiomyocyte cell line H9C2 was purchased from the American Type Culture Collection (Manassas, VA, USA) and was maintained in Dulbecco's modified Eagle's medium (DMEM) supplemented with 10% (v/v) FCS, l-glutamine (2 mM), streptomycin (100 μg/ml), and penicillin (100 IU/ml) (all from Gibco–Invitrogen Corp., UK). All cells were incubated in a humidified incubator at 37 °C and 5% CO_2. Cells were passaged at 80–90% confluence by trypsinization according to standard procedures. Cells cultured in normal growth medium at ~80% confluence were treated with the indicated concentrations of H_2O_2 (Sigma) for 20 min. For Src kinase inhibition, H9C2 cells at ~80% confluence were pretreated with PP1 (Alexis Biochemicals, San Diego, CA, USA) for 1 h before treatment with H_2O_2 or vehicle (ddH2O) for 20 min.

Immunoblotting and immunoprecipitation

For immunoblotting, cells were washed in chilled PBS and scraped in lysis buffer (50 mM Hepes, pH 7.4, 150 mM NaCl, 1% NP-40, 1 mM EDTA, 2 mM sodium orthovanadate, 100 μg/ml AEBSF, 17 μg/ml aprotinin, 1 μg/ml leupeptin, 1 μg/ml pepstatin, 5 μM fenvalerate, 5 μM BpVphen, and 1 μM okadaic acid). Lysates were clarified by centrifugation at $13,000 \times g$ for 30 min at 4 °C and protein concentra-

tions determined using the Coomassie protein assay reagent (Bio-Rad). Protein samples were diluted in Laemmli sample buffer (final concentrations: 50 mM Tris, pH 6.8, 10% (v/v) glycerol, 2% (w/v) SDS, 0.01% (w/v) bromophenol blue) and separated by one-dimensional (1D) SDS–PAGE according to standard procedures. Gel-separated proteins were electroblotted onto polyvinylidene difluoride membranes (Immobilon P; Millipore) in a transfer tank using transfer buffer (195 mM glycine, 25 mM Tris–HCl, 20% (v/v) methanol). Membranes were blocked for 30 min with 5% (w/v) bovine serum albumin in Tris-buffered saline (50 mM Tris, pH 8.0, 150 mM NaCl) with 0.1% Tween 20 (TBS-T). Membranes were incubated overnight with primary antibody solution in TBS-T. Membranes were washed in TBS-T (3×10 min) and then probed with the appropriate horseradish peroxidase-coupled secondary antibody (GE Healthcare). After further washes in TBS-T, immunoprobed proteins were visualized using the enhanced chemiluminescence method (Biovision). For small-scale immunoprecipitations, proteins were immunoprecipitated from 500 μg cell lysate using 5 μg antibody and 40 μl of a 50% slurry of protein A–Sepharose for 16 h at 4 °C. Immune complexes were then washed three times in lysis buffer and boiled in Laemmli sample buffer before immunoblot analysis.

Large-scale tyrosine-phosphorylated protein enrichment

Exponentially growing H9C2 cells (20×15-cm dishes; $\sim 10^8$ cells) were either left untreated or treated with 1 mM H_2O_2 for 20 min followed by washing in cold PBS and lysis in chilled modified RIPA buffer (50 mM Tris–HCl, pH7.4, 150 mM NaCl, 1% NP-40, 0.1% sodium deoxycholate, 1 mM EDTA plus protease inhibitors and 1 mM sodium orthovanadate). Lysates were precleared by incubation with 300 μl of protein A–agarose for 6 h at 4 °C on a rotator to reduce nonspecific binding during the immunoprecipitation. Subsequently, protein samples were incubated overnight with 300 μl of agarose-conjugated 4G10 anti-phosphotyrosine monoclonal antibody beads (Upstate). Immunoprecipitations were washed extensively with RIPA lysis buffer and proteins eluted with 1 bed volume of 150 mM phenyl phosphate. Samples were precipitated by adding 1 volume of 100% trichloroacetic acid (at -20 °C) to 4 volumes of sample with incubation for 10 min at 4 °C. Precipitated protein was recovered by centrifugation at $14,000 \times g$ for 5 min, and the pellet was washed twice with ice-cold acetone. Air-dried pellets were resuspended in 100 μl Laemmli sample buffer and boiled and proteins resolved by 12% 1D SDS–PAGE. Colloidal Coomassie Blue G-250 (CCB) staining using a modified version of the protocol by Neuhoff et al. [32] was used to visualize gel-separated proteins. Briefly, gels were fixed in 35% (v/v) ethanol with 2% (v/v) phosphoric acid overnight on a shaking platform and washed three times for 30 min each in ddH2O. They were then incubated in 34% (v/v) methanol, 17% (w/v) ammonium sulfate, and 3% (v/v) phosphoric acid for 1 h before the addition of 0.5 g/L Coomassie Blue G-250 (BDH) and left to stain for 2–3 days. Poststained gels were imaged on an ImageScanner III densitometer (GE Healthcare).

In-gel digestion

Excised poststained gel pieces were washed three times in 50% acetonitrile, dried in a SpeedVac for 10 min, reduced with 10 mM DTT in 5 mM ammonium bicarbonate, pH 8. 0 (AmBic), for 45 min at 50 °C, and then alkylated with 50 mM IAM in 5 mM AmBic for 1 h at room temperature in the dark. Gel pieces were then washed three times in 50% acetonitrile and vacuum-dried before reswelling with 50 ng of modified trypsin (Promega) in 5 mM AmBic. The pieces were then overlaid with 10 μl of 5 mM AmBic and trypsinized overnight at 37 °C. Supernatant was collected and peptides were further extracted twice with 5% trifluoroacetic acid in 50% acetonitrile and the supernatants pooled. Peptide extracts were vacuum-dried

and resuspended in 5 µl ddH$_2$O containing 0.1% formic acid and stored at −20 °C before liquid chromatography (LC)–MS/MS analysis or matrix-assisted laser desorption ionization time-of-flight (MALDI-TOF) MS analysis.

Liquid chromatography and tandem mass spectrometry

LC–MS/MS was performed by injecting 5 µl of digested peptides onto a reversed-phase capillary column using a nanoflow HPLC system (Agilent 1200 Nanoflow LC) connected online to an ESI Q-TOFI mass spectrometer (Waters, UK). The flow rate was 300 nl/min and separation was performed by gradient elution from 5 to 50% solution B (80% (v/v) acetonitrile, 0.1% formic acid) in 60 min followed by an isocratic step at 100% solution B for 10 min. Balance solution A was 0.1% formic acid. Data-dependent acquisition was used with MS scans set every second (m/z 500–1500) and MS/MS performed on automatically selected peptide ions, also for 1 s (m/z 50–2000, continuum mode), using the function switching in MassLynx version 4.0 software.

Raw MS/MS data were smoothed (Savitzky Golay, two channels twice) and centroided (at 80%) and peak lists generated using MassLynx software. Peak lists were submitted for database searching using Mascot (version 2.2.04). Parameters for protein searches were enzyme trypsin, porcine; miscleavages 2; charge of ions +2 and +3; SwissProt/TrEMBL database release version 55.1, 359,942 sequence entries; species *Rattus*; mass tolerance of precursor peptide ion 100 ppm; and mass tolerance for MS/MS fragment ions 0.8 mmu. Carbamidomethylation of cysteines was considered a fixed modification, whereas oxidation of methionine, pyroglutamic acid, and *N*-acetylation and phosphorylation of tyrosine, serine, and threonine were considered variable modifications.

Protein identification by MALDI-TOF MS

MALDI-TOF MS by peptide mass fingerprinting was also used for protein identification. Briefly, 0.5 µl of tryptic digest was mixed with 0.5 µl of matrix solution containing α-cyano-4-hydroxycinnamic acid at a concentration of 1 mg/ml in 50% acetonitrile (v/v)/0.1% trifluoroacetic acid (v/v) and spotted onto an anchorchip target plate (Bruker Daltonics) and air dried. The peptide mass fingerprints were acquired on an Autoflex III mass spectrometer (Bruker Daltonics) in the reflector mode. The spectrometer was calibrated with peptide calibration standard (Bruker Daltonics) and internal calibration was performed using trypsin autolysis peaks at m/z 842.51 and m/z 2211.1046. Peaks in the mass range m/z 600–4000 were used to generate a peptide mass fingerprint, which was searched against the updated SwissProt/TrEMBL database (release version 57.9; 510,076 sequence entries) using Mascot software version 2.2.06 (Matrix Science, London, UK) and the following parameters: *Rattus*, tryptic digest with a maximum of 1 missed cleavage, carbamidomethylation of cysteine, partial protein N-terminal acetylation, partial methionine oxidation and partial modification of glutamine to pyroglutamate, and a mass tolerance of 100 ppm. Identifications were accepted based on significant Mascot Mowse scores ($p < 0.05$), a minimum of six peptide masses matching a particular protein, spectrum annotation, and observed versus expected molecular weight and p*I* on 2D gels.

Immunostaining and fluorescence microscopy

For immunofluorescence staining, H9C2 cells plated on coverslips were pretreated with 5 µM PP1 or vehicle for 1 h before treatment with 1 mM H$_2$O$_2$ or vehicle for 20 min. Cell were fixed with 4% paraformaldehyde for 25 min and the attached cells washed twice with PBS. Localization of selected proteins was assessed using primary antibody diluted in 2.5% BSA/PBS and incubated with cells

at room temperature for 1 h. After three PBS washes, samples were incubated with appropriate fluorescently labeled secondary antibodies diluted in 2.5% BSA/PBS. For localization of filamentous actin, cells were incubated with 0.1 µg/ml Alexa 568–phalloidin (Sigma) for 45 min at 37 °C. Coverslips were then washed three times with PBS and at least twice with ddH$_2$O before being mounted in Vectashield mounting medium (Vector Laboratories). Coverslip edges were sealed with nail polish onto glass slides (BDH) and dried in the dark at 4 °C. For image analysis, cells were imaged using a Zeiss Axiovert 200 M fluorescence microscope (Carl Zeiss, Germany). All laser intensities used to detect the same immuno-stained markers were the same and all laser intensities used for capturing images were not saturated. Images were exported as .tif files using Zeiss Axioversion 4.0 and processed using Adobe Photo-shop version 7.0 software.

Adhesion assays

H9C2 cells (5000 cells/well) pretreated with 5 µM PP1 or vehicle (for 1 h) followed by 1 mM H$_2$O$_2$ for 20 min were added to wells in DMEM containing 10% FCS. Cells were left to adhere for the indicated times at 37 °C in a 5% CO$_2$ humidified incubator. The assay was terminated by aspirating the cell suspension and gently washing the wells three times with PBS to remove unbound or loosely attached cells. Substratum-bound cells were counted by microscopy. All conditions were repeated six times.

MTT cell viability assay

H9C2 cells growing exponentially were trypsinized and counted using a hemacytometer and 5000 cells/well were seeded into 96-well plates. The culture was then incubated for 24 h before pretreatment with 5 µM PP1 for 1 h and then 1 mM H$_2$O$_2$ for 20, 60, and 240 min or left untreated. After removal of the medium, 50 µl of MTT working solution (1 mg/ml; Sigma) was added to the cells in each well, followed by a further incubation at 37 °C for 4 h. The supernatant was carefully removed. One hundred microliters of dimethyl sulfoxide (DMSO) was added to each well and the plates were shaken for 20 min. The absorbance of the samples was then measured at a wavelength of 540 nm in a multiwell plate reader. Values were normalized against the untreated samples and were averaged from four independent measurements.

Apoptosis assay

H9C2 cells growing exponentially were pretreated with 5 µM PP1 or vehicle (for 1 h) followed by 1 mM H$_2$O$_2$ for 20 min and then were trypsinized and fixed with 4% paraformaldehyde in PBS for 20 min. The suspension was centrifuged at 1500 rpm for 5 min, incubated with 50 µl of 5% BSA solution to reduce nonspecific binding, and centrifuged again. The cell samples were resuspended with appropriate amounts of annexin V labeling solution according to the manufacturer's protocol (Millipore) before fluorescence-activated cell sorting was performed. In all experiments, 10,000 cells were analyzed. Analysis of cellular events was performed using FACSCalibur with CellQuest software (Becton–Dickinson). All analyses were carried out on at least three independent occasions.

2D-DIGE and gel image analysis

For performing 2D-DIGE, protein samples were labeled with *N*-hydroxysuccinimidyl ester derivatives of the cyanine dyes Cy2, Cy3, and Cy5 following the protocol described previously [33–35]. Briefly, 150 µg of protein sample lysed in 2D lysis buffer (7 M urea, 2 M thiourea, 4% Chaps, 0.5% NP-40) was minimally labeled with 375 pmol of either Cy3 or Cy5 for comparison on the same 2D gel.

A pool of all samples was also prepared and labeled with Cy2 at the same molar ratio of 2.5 pmol Cy2/µg protein as an internal standard to be run on all gels to facilitate image matching and cross-gel statistical comparison. Labeling reactions were performed in the dark on ice for 30 min and then quenched with a 20-fold molar excess of free l-lysine to dye for 10 min. The differentially Cy3- and Cy5-labeled samples were mixed with the Cy2-labeled internal standard and reduced with DTT for 10 min. IPG buffer, pH 3–10, nonlinear (2% (v/v); GE Healthcare) was added and the final volume was adjusted

to 450 µl with 2D lysis buffer. Immobilized nonlinear pH gradient (IPG) strips (pH 3–10, 24 cm) were rehydrated with the Cy-labeled samples in the dark at room temperature overnight (at least 12 h). Isoelectric focusing was then performed using a Multiphor II apparatus (GE Healthcare) for a total of 62.5 kVh at 20 °C. Strips were equilibrated in 6 M urea, 30% (v/v) glycerol, 1% SDS (w/v), 100 mM Tris–HCl (pH 8.8) with 65 mM DTT for 15 min and then in the same buffer containing 240 mM IAM for 15 min. The equilibrated IPG strips were transferred onto 24×20-cm 12.5% polyacrylamide
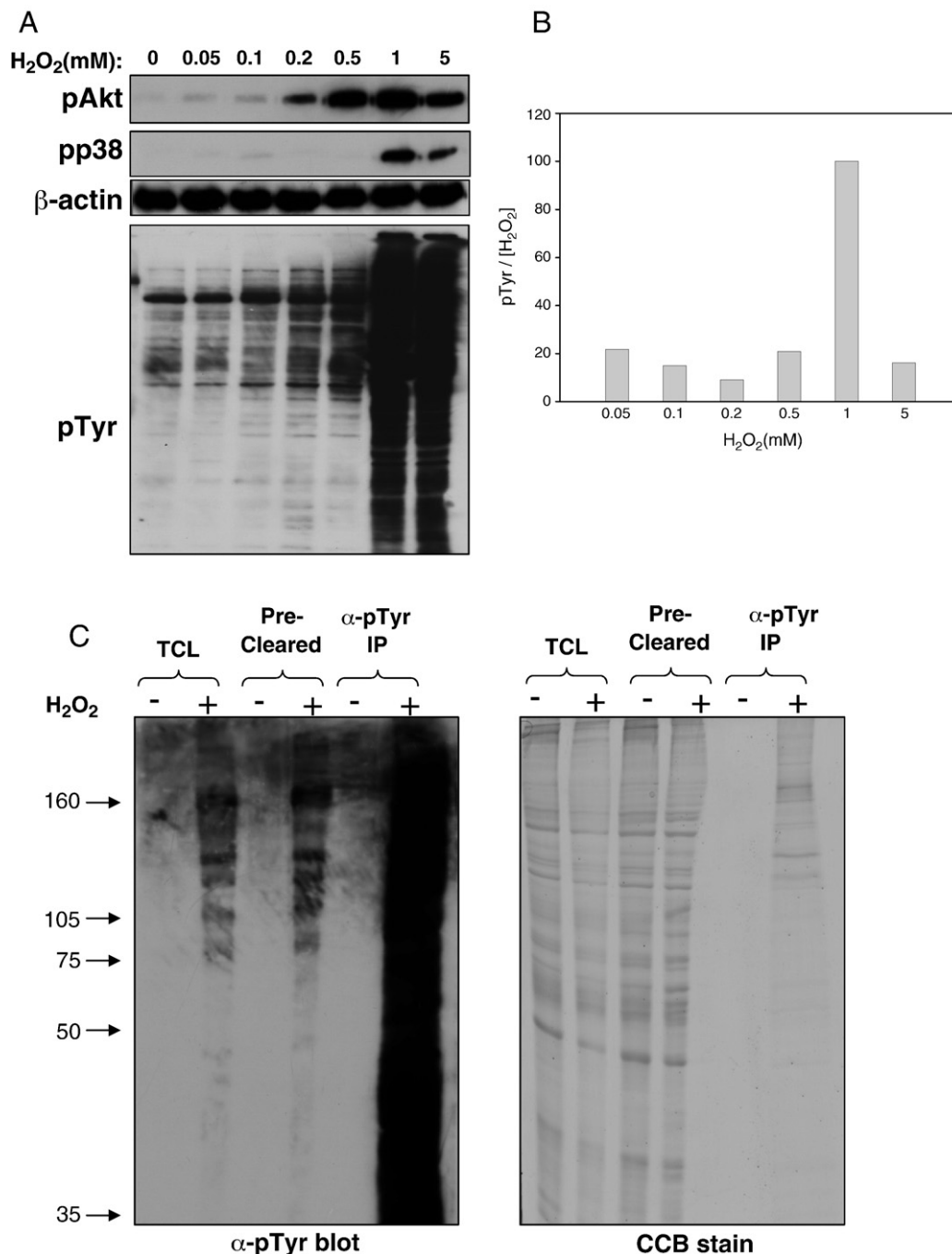
Fig. 1. Effect of hydrogen peroxide treatment on signaling in H9C2 cells and purification of tyrosine-phosphorylated proteins. (A) Total cell lysates (TCL) were prepared from H9C2 cells treated with hydrogen peroxide at the indicated concentrations for 20 min. Total protein (30 µg) was separated by 1D SDS–PAGE, electrophoretically transferred onto an Immobilon P membrane, and probed with specific antibodies to the indicated proteins and phosphorylation motifs. (B) The ratio of protein phosphorylation to the concentrations of H_2O_2 based on the intensity of pTyr and the concentration of H_2O_2 used for treatment was calculated. (C) H9C2 cells were either left untreated or treated with 1 mM H_2O_2 for 20 min followed by preclearing with protein A and enrichment with anti-phosphotyrosine mouse monoclonal antibody (4G10). 10 µg of TCL, 10 µg of protein A precleared lysate, 1 µg of affinity-purified protein from untreated cells, and 3 µg of affinity-purified protein from H_2O_2-treated cells were resolved by 1D SDS–PAGE followed by immunoblotting with anti-phosphotyrosine antibody pY99 (left) and visualization of proteins by CCB staining (right).

gels cast between low-fluorescence glass plates. Gels were bonded onto the inner plates using bind-saline solution (GE Healthcare). The strips were overlaid with 0.5% (w/v) low-melting-point agarose in running buffer containing bromophenol blue. The gels were run in an Ettan 12 gel tank (GE Healthcare) at 4 W per gel at 10 °C until the dye front had completely run off the bottom of the gels. 2D-DIGE gels were scanned directly between the low-fluorescence glass plates using an Ettan DIGE imager (GE Healthcare). Image analysis was performed using DeCyder 2-D Differential Analysis software version 7.0 (GE Healthcare) to codetect, normalize, and quantify the protein features in the images. Features detected from non-protein sources (e.g., dust particles and dirty background) were filtered out. Protein spots displaying a >1.5-fold average increase or decrease in abundance with p value <0.05 were selected for protein identification.

Results

Hydrogen peroxide treatment induces tyrosine phosphorylation and activation of PI3K and stress response signaling pathways in H9C2 cardiomyocytes

ROS play important roles in the transmission and regulation of cellular signaling. The most notable effect of ROS on cell signaling is the induction of tyrosine phosphorylation resulting from the oxidative modification and inhibition of protein tyrosine phosphatases. In this study, we examined the targets of ROS-induced tyrosine phosphorylation in H9C2 rat cardiomyocytes, as it is a widely used cell model for examining the mechanisms of heart ischemia–reperfusion injury and antioxidant protection. In preliminary experiments we examined a range of doses of H_2O_2 treatment to find a maximal

Table 1
Proteins identified in large-scale anti-phosphotyrosine immunoprecipitation from H_2O_2-treated H9C2 cells

SwissProt Acc. No.	Protein name	Gel MW	Pred MW	Pred pI	No. matched peptides	Coverage (%)	Score	Matched peptides	Functional distribution
P62738	Actin, aortic smooth muscle	45,000	42,381	5.23	2	9	54/34	SYELPDGQVITIGNER; YPIEHGIITNWDDMEK	Cytoskeleton/adhesion/ motility regulation
P00762	Anionic trypsin-1	30,000	26,627	4.71	2	10	36/34	LGEHNINVLEGDEQFINAAK; LSSPVK	Secretion
P26231	Catenin-α1	120,000	102,220	6.49	4	4	104/42	GYELLFQPEVVR; HAIPNLVK	Cytoskeleton/adhesion/ motility regulation
Q9WU82	Catenin-β1	105,000	86,027	5.53	2	3	66/34	LHYGLPVVVK; NEGVATYAAAVLFR	Cytoskeleton/adhesion/ motility regulation
P30999	Catenin-δ1	105,000	102,220	6.49	4	4	127/43	HAIPNLVK; AAALVLQTIWGYK	Cytoskeleton/adhesion/ motility regulation
Q66HL2	Cortactin-Src substrate/CTTN	75,000	57,078	5.11	15	26	126/37	VDKSAVGFEYQGK; YGLFPANYVELR	Cytoskeleton/adhesion/ motility regulation
Q6IMF3	Cytokeratin-1	160,000[a]	65,190	8	3	5	129/44	SLNDKFASFIDK; FLEQQNQVLQTK	Cytoskeleton/adhesion/ motility regulation
Q6IFV3	Cytokeratin-15	160,000[a]	49,011	4.8	2	3	93/33	LASYLDK; VTMQNLNDR	Cytoskeleton/adhesion/ motility regulation
Q4FZU2	Cytokeratin-6A	160,000[a]	59,555	8.06	3	3	100/33	YEELQITAGR; SLDLDSIIAEVK	Cytoskeleton/adhesion/ motility regulation
Q6IG03	Cytokeratin-73	60,000	60,977	8.17	2	2	88/34	FLEQQNQVLQTK; NLDLDSIIAEVR	Cytoskeleton/adhesion/ motility regulation
Q6IG05	Cytokeratin-75	160,000[a]	62,472	7.6	3	6	79/37	SLDLDSIIAEVK; LVELEDALQKAK	Cytoskeleton/adhesion/ motility regulation
P62630	Elongation factor-1α1	50,000	50,424	9.1	2	3	40/34	RYEEIVK; STTTGHLIYK	Protein translation
P54761	Ephrin type-B receptor-4	120,000	110,198	6.53	2	2	115/42	FPQVVSALDK; APSGAVLDYEVK	Development
O35346	Focal adhesion kinase-1[b]	120,000	119,717	6.24	2	3	72/33	NLLDVIDQAR; LLNSDLGELISK[b]	Cytoskeleton/adhesion/ motility regulation
P70600	Focal adhesion kinase-2/PTK2b[b]	120,000	115,784	6.24	2	2	102/42	NLLDVIDQAR; LLNSDLGELISK[b]	Cytoskeleton/adhesion/ motility regulation
Q62847	γ-Adducin	75,000	79,097	5.46	2	3	37/35	IELQKVLGPSCK; NGETpSPR	Cytoskeleton/adhesion/ motility regulation
Q6P0K8	Junction plakoglobin	90,000	81,749	5.75	3	4	81/33	LLNDEDPVVVTK; ALMGSPQLVAAVVR	Cytoskeleton/adhesion/ motility regulation
Q75NI5	M-cadherin	120,000	85,929	4.62	2	2	38/37	DPDTEQLQR; FTILEGDPDGQFK	Cytoskeleton/adhesion/ motility regulation
Q63767	p130CAS/breast cancer anti-estrogen resistance protein-1	120,000	104,540	5.9	6	6	157/33	KGDIMTVLER; TKAPGPGPEGSSSLHLNPTDK	Cytoskeleton/adhesion/ motility regulation
Q05030	Platelet-derived growth factor receptor-β	160,000	123,833	5.03	3	3	142/43	HVDQPLSVR; TLGDSSAGELVLSTR	Growth regulation
P69897	Tubulin-β5	50,000	50,095	4.78	3	8	35/34	IREEYPDR; AILVDLEPGTMDSVR	Cytoskeleton/adhesion/ motility regulation
Q5FWT7	Ubiquitin-like domain-containing CTD phosphatase-1	50,000	36,957	6.07	2	5	51/35	pSLPIIVK; VEVLNPPR	Cell signaling
P31977	Villin-2/ezrin	85,000	69,348	5.83	2	4	56/33	SQEQLAAELAEYTAK; IQVWHAEHR	Cytoskeleton/adhesion/ motility regulation

H_2O_2-induced tyrosine-phosphorylated proteins were affinity purified using agarose-conjugated anti-phosphotyrosine mouse monoclonal antibody (4G10) and recovered using a phenyl phosphate elution step and acetone precipitation. Proteins were separated by 1D SDS–PAGE and stained bands excised and trypsin digested. Extracted peptides were further separated and analyzed by LC–MS/MS (Q-TOF) and identified by Mascot database searching. All identified proteins are shown, organized by name with Swiss-Prot accession number, approximate gel-based MW, predicted MW, predicted pI, the number of peptides matching the database sequence, the sequence coverage (%), the Mascot database search score (denominator is score at $p = 0.05$), matching peptide sequences, and functional distribution.

[a] Proteins showing disagreement in gel-based and predicted molecular weights.

[b] The two identified proteins contained identical matched peptides and cannot be discriminated in this experiment, although both were detected in anti-pY immunoprecipitates by immunoblotting (see Fig. 4C).

response in terms of tyrosine phosphorylation as assessed by immunoblotting. The results indicated that concentrations of 1–5 mM H_2O_2 gave a robust though transient increase in tyrosine phosphorylation (Fig. 1A). The ratio of protein phosphorylation to the concentration of H_2O_2 based on the intensity of pTyr and the concentration of H_2O_2 used for treatment in Fig. 1A was calculated and the result indicated that H_2O_2 induced a maximal pTyr/[H_2O_2] at 1 mM H_2O_2, implying this is the optimal concentration to induce adequate phosphorylation signals in H9C2 cells for research (Fig. 1B). At 10 mM H_2O_2, most cells became detached from the substratum (data not shown). Notably, 1 mM H_2O_2 treatment for 20 min also resulted in maximal activation of Akt and p38 (Fig. 1A). These results show that H_2O_2-induced oxidative stress can activate cell signaling pathways and thus is likely to play a role in regulating cellular stress responses, proliferation, survival, and differentiation.

Identification of hydrogen peroxide-induced tyrosine-phosphorylated proteins

To enrich the H_2O_2-induced tyrosine phosphorylated proteins for protein identification, a large-scale immunoprecipitation approach was performed using agarose-conjugated anti-phosphotyrosine antibody and a phenyl phosphate elution step. The enrichment process started with 10^8 cells (30 mg total protein) with a purification yield of 60 μg (0.2% of total) from H_2O_2-treated H9C2 cells (1 mM; 20 min) and 5 μg (0.016% of total) from untreated cells. The purified tyrosine-phosphorylated proteins were then resolved by 1D SDS–PAGE (Fig. 1C) and CCB-stained bands were subsequently excised and digested with trypsin and submitted for identification by LC–MS/MS. A total of 23 proteins were identified with high confidence (Table 1), including platelet-derived growth factor receptor-β and γ-adducin (Fig. 2). Only 3 unique proteins were identified from the untreated cells, in which the basal tyrosine phosphorylation levels were low, demonstrating the effectiveness of the strategy. These proteins were all abundant proteins not normally known to be tyrosine phosphorylated (tubulin-β, HSP60, and actin) and might be coprecipitated as a result of nonspecific binding (data not shown). The identified proteins were functionally annotated from SwissProt database searches and most (18 of 23) are reported to be associated with the cytoskeleton (actin, cytokeratin-1, cytokeratin-15, cytokeratin-6A, cytokeratin-73, cytokeratin-75, tubulin-β5), focal adhesions (focal adhesion kinase-1, focal adhesion kinase-2), cell–cell and cell–matrix adhesion (catenin-
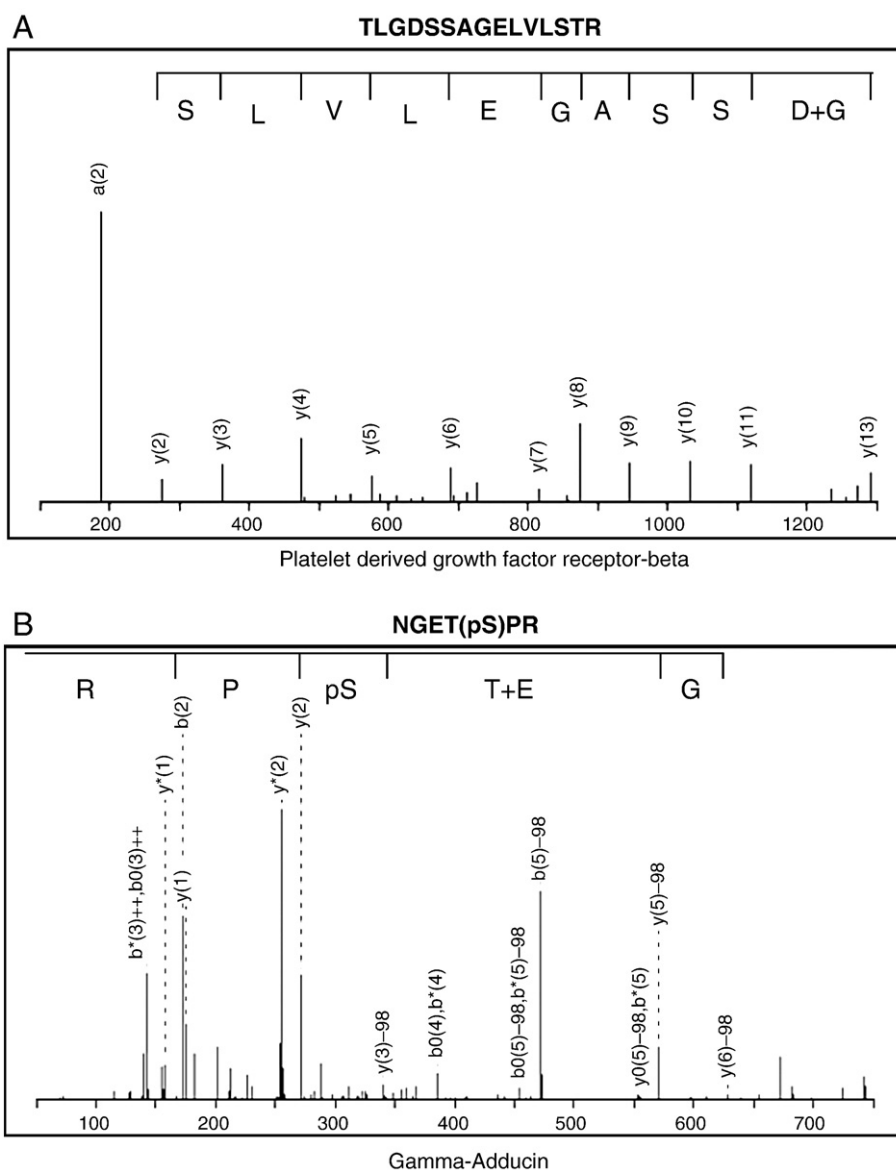
Fig. 2. MS/MS spectra of identified peptides. MS/MS fragmentation spectra and sequence of (A) the platelet-derived growth factor receptor-β peptide TLGDSSAGELVLSTR and (B) the γ-adducin peptide NGET(pS)PR.
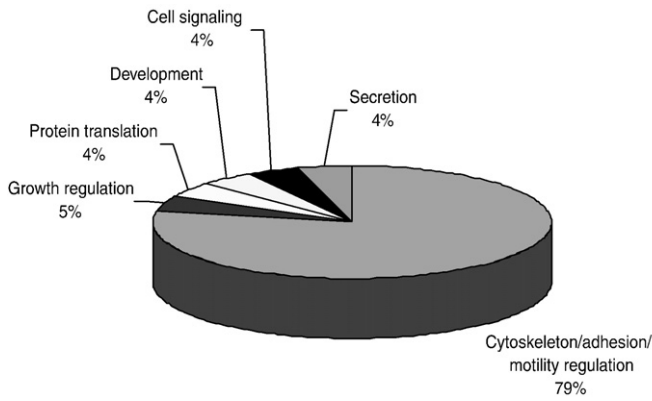
Fig. 3. Functional distribution of the identified H_2O_2-induced tyrosine-phosphorylated proteins.

α1, catenin-β1, catenin-δ1, cortactin-Src substrate, ezrin, γ-adducin, junction plakoglobin, M-cadherin, and p130CAS/breast cancer anti-estrogen resistance protein-1) (Fig. 3 and Table 1). These data suggest that H_2O_2 and the tyrosine phosphorylation it induces may have profound effects on the cytoskeleton, adhesion, and/or cell–cell connections. Notably, even though numerous cytokeratins were identified, all sequences were specific to *Rattus norvegicus* and not *Homo sapiens,* confirming that these were not due to contamination.

Role of Src kinases in H_2O_2-induced tyrosine phosphorylation

A substantial portion of the proteins identified have been reported to be associated with the Src kinase, including catenin-α1 [36], catenin-β1 [37], cortactin-Src substrate [38], focal adhesion kinase-2 (FAK2) [39], breast cancer anti-estrogen resistance protein-1 [40], platelet-derived growth factor receptor-β (PDGFRβ) [41], and focal adhesion kinase-1 [42]. Therefore we investigated whether Src kinase
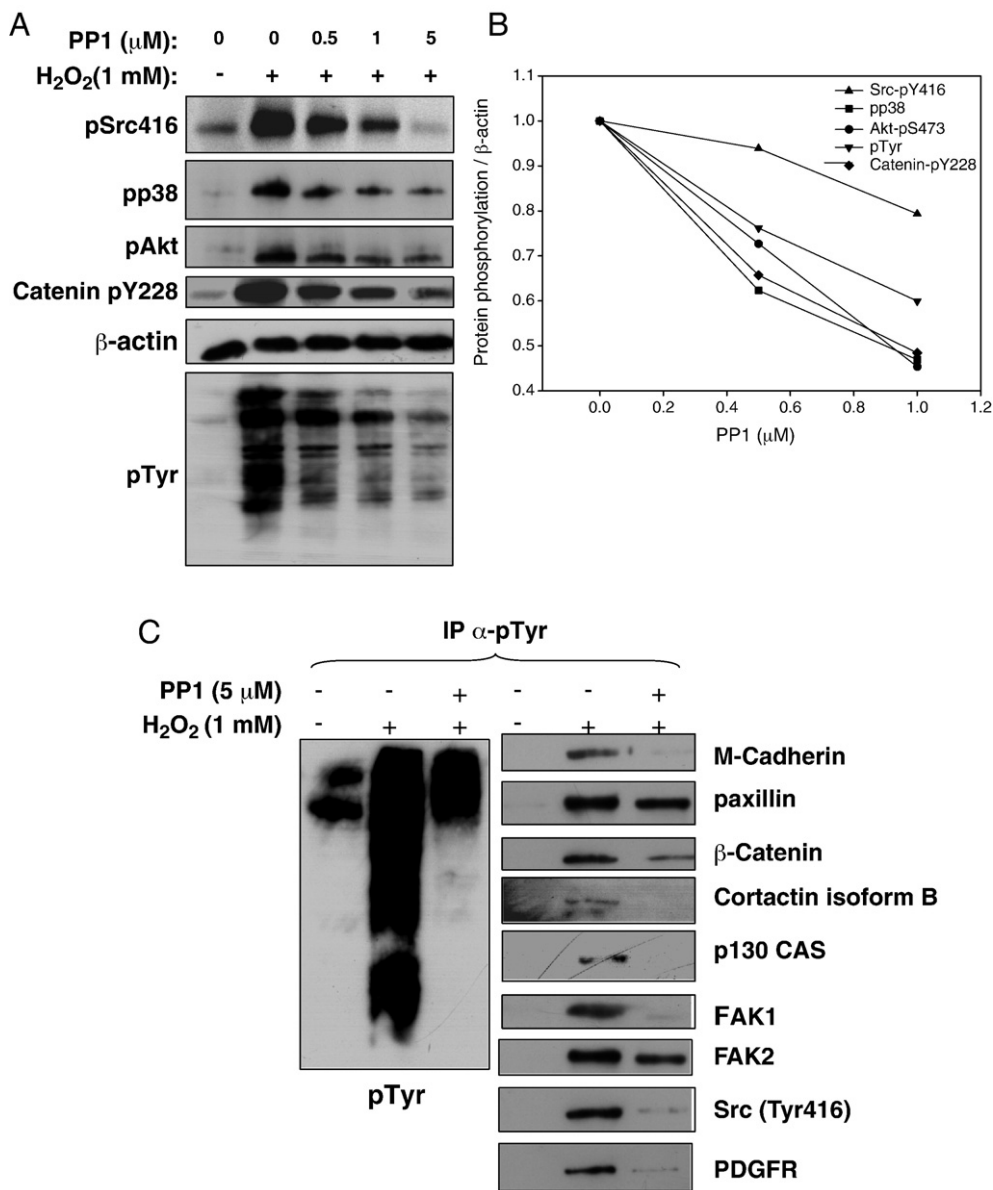
Fig. 4. Effect of Src kinase inhibitor, PP1, on H_2O_2-induced signaling events and tyrosine-phosphorylated protein recovery. (A) Total cell lysates prepared from untreated and treated H9C2 cells were immunoblotted with antibodies against the indicated phosphorylated proteins and the loading control, β-actin. Cells were left untreated or pretreated with the indicated concentrations of Src kinase inhibitor PP1 for 1 h, before treatment with 1 mM H_2O_2 for 20 min. (B) The relative band densities of pSrc416, pp38, pAkt, catenin pY228, and pTyr were normalized to actin and then against the PP1 concentrations. (C) Affect of Src kinase inhibition on recovery of tyrosine-phosphorylated proteins. Small-scale anti-phosphotyrosine immunoprecipitations from untreated and PP1-pretreated and H_2O_2-treated cells were immunoblotted for the indicated proteins.

plays a role in mediating H_2O_2-induced tyrosine phosphorylation events in these cells. To address this, a Src kinase inhibitor, PP1, was used to examine the effects of reducing Src kinase activity after H_2O_2 treatment. H9C2 cells were pretreated with the indicated concentrations of PP1 for an hour followed by treatment with 1 mM H_2O_2 for 20 min, and tyrosine phosphorylation was monitored by immunoblotting. The results showed that PP1 could significantly reduce H_2O_2-induced tyrosine phosphorylation, implicating Src kinase as a major mediator of peroxide-induced phosphorylation (Fig. 4A). Src kinase was activated in response to H_2O_2 treatment as indicated by phosphorylation at Y416 in the active site, which was reduced by PP1 treatment. In addition, PP1 treatment also reduced catenin, Akt, and p38 activation in response to H_2O_2, suggesting an upstream role for Src kinase in mediating the activation of known adhesion, survival, and stress-activated signaling pathways in response to oxidative stress (Fig. 4A). Further analysis by normalization of the relative band densities of pSrc416, pp38, pAkt, pY228 catenin, and pTyr to actin

demonstrated that there is a dose-dependent response to PP1 for all of these proteins (Fig. 4B). PP1 pretreatment also resulted in the loss of proteins and/or their tyrosine phosphorylation in anti-phosphotyrosine immunoprecipitations from H_2O_2-treated cells, including M-cadherin, paxillin, β-catenin, cortactin B, p130CAS, FAK1, FAK2, and PDGFR (Fig. 4C). Taken together, these results suggest a direct role for the Src kinase in mediating the cellular responses to oxidative stress.

Role of Src kinase in hydrogen peroxide-induced loss of cell adhesion and viability

The high proportion of proteins identified with roles in cellular adhesion and cytoskeletal regulation prompted us to examine the effect of H_2O_2 treatment on the actin cytoskeleton, cell–cell interactions, and cell–substratum adhesion events. Using immunofluorescence staining, the robust increase in tyrosine phosphorylation in
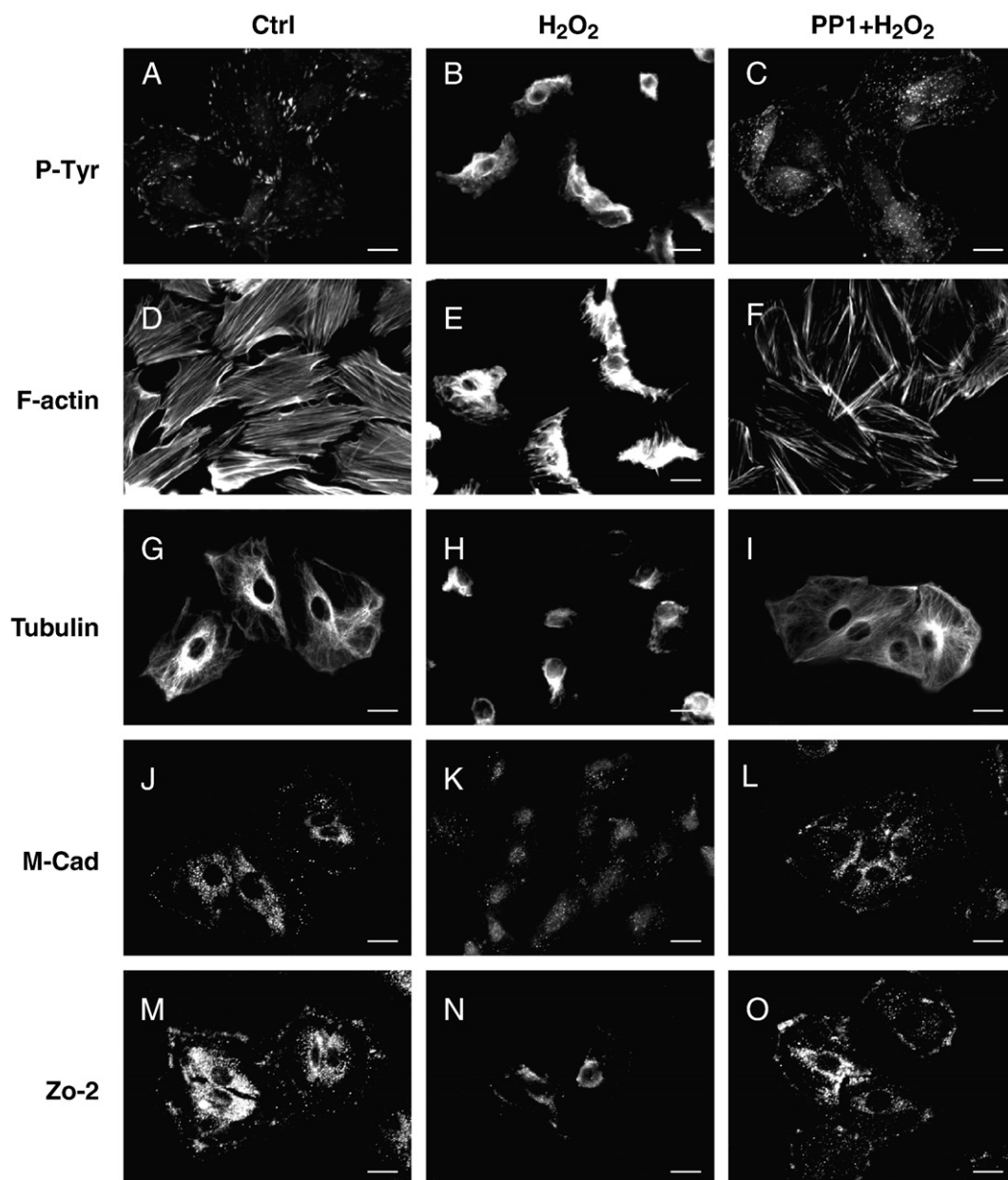
Fig. 5. Immunofluorescence analysis of morphological and protein localization changes in H9C2 cells in response to H_2O_2 treatment and pretreatment with PP1. H9C2 cells on coverslips were either left untreated or treated with 1 mM H_2O_2 for 20 min or pretreated with 5 μM PP1 for 1 h and then with H_2O_2 for 20 min before fixation and staining for pTyr, F-actin, tubulin, M-cadherin, and ZO-2. Each set of three fields was taken using the same exposure, and images are representative of six different fields. Scale bar, 20 μm.

response to H_2O_2 was first confirmed, as was its potent inhibition by PP1 pretreatment (Figs. 5A–C). Tyrosine phosphorylation was primarily localized to the cell cytoplasm and regions of cell–substratum contacts (focal adhesions) in untreated H9C2 cells, though cells were very heavily stained in all but the nuclei of H_2O_2-treated cells. H_2O_2 treatment also resulted in modification of the actin cytoskeleton and tubulin with more diffuse staining of cytoplasmic filamentous actin and tubulin, loss of stress fibers, and loss of uniform cell shape (Figs. 5D–I). These changes could be partially rescued by pretreatment of cells with PP1. Expression of the homotypic cell–cell adhesion protein M-cadherin was localized predominantly to regions

of cell–cell contact in untreated cells (Fig. 5J). This localized staining was lost in response to H_2O_2, but could be rescued by pretreatment with the PP1 inhibitor (Figs. 5J–L). Similarly, staining for the tight-junction protein ZO-2 revealed more intense staining in areas of cell–cell contact, presumably representing tight junctions, and this staining was significantly reduced in H_2O_2-treated cells and restored by PP1 pretreatment (Figs. 5M–O). Together, these data indicate that oxidative stress in cardiomyocytes results in a significant alteration of the actin cytoskeleton and changes in cell morphology, with a substantial loss of normal cell–cell contacts, and that Src activation is a major regulator of these events.

We next examined the effect of peroxide and Src kinase inhibition on cell adhesion itself using a simple adhesion assay. H9C2 cells that were untreated, treated with peroxide alone, or pretreated with PP1 and then peroxide were plated for 1 or 4 h followed by gentle washing with PBS to remove unbound cells, and the remaining adherent cells were counted. The results showed that H_2O_2 treatment significantly reduced the adhesive capacity of the cells and that this could be partially rescued by PP1 pretreatment (Fig. 6A). This suggests that peroxide-induced Src activation decreases the adhesive capability of cardiomyocytes. Further experiments to determine the effect of peroxide on cell viability were performed using an MTT assay. Cell viability was decreased to about 75% after 20 min, 50% after 1 h, and 20% after 4 h of H_2O_2 treatment, whereas PP1 pretreatment resulted in the maintenance of about 95, 85, and 60% of viability/adhesion after 20 min, 1 h, and 4 h of treatment, respectively (Fig. 6B). This suggests that Src-dependent signaling may also play a role in mediating peroxide-induced cell death, as well as cell adhesion. To further explore a possible role of Src activation in peroxide-induced cell apoptosis, the apoptotic marker annexin V was examined by fluorescence-activated cell sorting of fixed cells. In response to peroxide treatment, there was an increase in annexin V staining from 31 to 91%, presumably reflecting its exposure at the cell surface in response to H_2O_2 treatment (Fig. 6C). When cells were pretreated with PP1 before H_2O_2 exposure, cell surface annexin V staining was reduced to 67% a level between those of untreated and H_2O_2-treated cells (Fig. 6C). These data suggest that blocking Src kinase activity can suppress and protect H9C2 cells from oxidative damage-induced apoptosis, which may be caused by the observed tyrosine hyperphosphorylation.

Global protein expression analysis of untreated and H_2O_2-treated H9C2 cells with and without PP1 pretreatment

To better understand the cardiomyocyte response to H_2O_2 treatment and the role of Src kinase in mediating oxidative stress signaling, a 2D-DIGE experiment was performed to examine the protein expression changes in H_2O_2-treated, PP1-pretreated, and
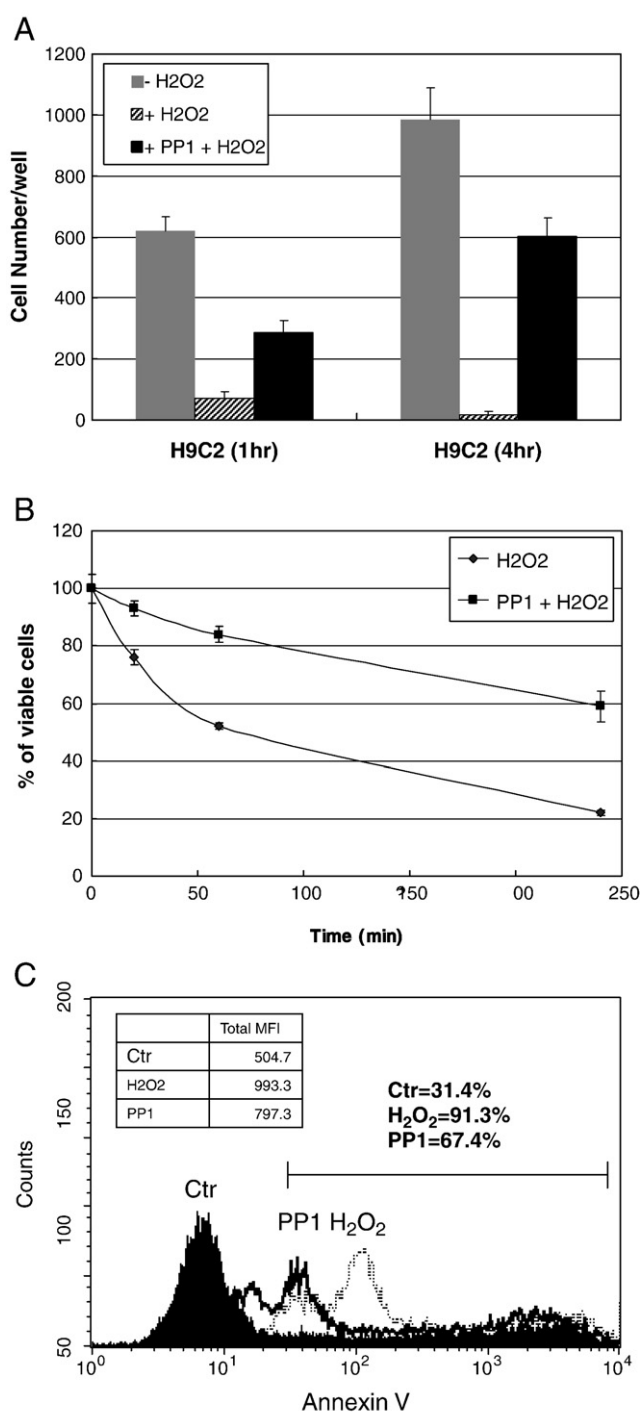
Fig. 6. Effects of H_2O_2 and Src kinase inhibitor on H9C2 cell adhesion, viability, and apoptosis. (A) Adhesion assays were performed in which 5000 cells pretreated with PP1 and/or H_2O_2 or left untreated were plated into 96-well plates in medium containing 10% FCS at 37 °C. After 1 and 4 h, cells were gently washed three times and the number of adherent cells was counted using a hemacytometer. The average of six independent assays ± the standard deviation is shown. (B) MTT-based viability assays were performed in which 5000 H9C2 cells were plated into 96-well plates in medium containing 10% FCS. After 24 h, the cells were pretreated with 5 μM PP1 for 1 h followed by treatment with 1 mM H_2O_2 for 20 min and 1 and 4 h or were left untreated. Cells were incubated with MTT and then DMSO was added and the plates were shaken for 20 min followed by measurement of the absorbance at 540 nm. Values were normalized against the untreated samples and are the averages of eight independent measurements ± the standard deviation. (C) H9C2 cells growing exponentially were either left untreated or treated with 1 mM H_2O_2 for 20 min or pretreated with PP1 for 1 h and then treated with H_2O_2 for 20 min before fixation with 4% paraformaldehyde in PBS for 25 min. Cell samples were resuspended with appropriate amounts of annexin V labeling solution before fluorescence-activated cell sorting was performed. In all experiments, 10,000 cells were analyzed. All analyses were carried out on at least three independent occasions.

untreated H9C2 cells. The analysis revealed more than 80 protein features that displayed differential expression (>1.5-fold; $p<0.05$) between the three conditions (Fig. 7A). Proteins in 38 of these features were subsequently identified by MALDI-TOF MS (Table 2). These differentially expressed proteins mostly have functions in metabolic regulation, cell motility, and stress responses. Notably, 23 of the 38 identified proteins showed H_2O_2-dependent changes that were at least partially reversed by PP1 pretreatment (Table 2, italic type). For example, protein spot 1251 (glutathione *S*-transferase Mu 5), was 4.85-fold down-regulated by H_2O_2 treatment, but did not change as dramatically (-1.82-fold) when cells were pretreated with PP1 (Fig. 7B). In addition, protein spot 1255, identified as heat shock protein-β1/Hsp27, was 3.9-fold down-regulated by H_2O_2 treatment, but did not change significantly (-1.11-fold) between the PP1 plus

Fig. 7. Proteomic comparison in H9C2 cells in response to H_2O_2 treatment and pretreatment with PP1. (A) Protein samples (150 μg each) purified from total cell lysates were labeled with Cy dyes and separated using 24-cm, pH 3–10 nonlinear IPG strips. The differentially expressed protein features are annotated with spot numbers. (B) Representative image of protein spot 1251 displaying H_2O_2- and PP1-dependent protein expression changes.

Table 2
Alphabetic list of identified differentially expressed proteins after 2D-DIGE coupled with MALDI-TOF mass spectrometry analysis in H9C2 cells in response to H_2O_2 treatment and pretreatment with PP1

Spot No.	SwissProt No.	Protein name	Pred MW	Pred pI	Score	No. peptide matches/supplied	Cov. (%)	H_2O_2/Ctrl[a]	PP1 + H_2O_2/Ctrl[a]
1420	P63324	40 S ribosomal protein S12	14,858	6.82	55/51	6/30	42	**−1.25**	**−6.4**
691	Q9JLJ3	4-Trimethylaminobutyraldehyde dehydrogenase	54,530	6.57	109/56	16/66	44	1.68	1.95
473	P63039	60-kDa heat shock protein (mitochondrial)	61,088	5.91	61/56	8/30	20	1.37	1.64
990	P54921	α-Soluble NSF attachment protein	33,627	5.3	120/56	13/39	50	*9.85*	*5.98*
1002	P55260	Annexin A4	36,168	5.31	145/51	13/28	39	−1.92	−2.01
1116	P35426	Cell division protein kinase-4	34,006	6.09	198/56	15/32	54	*3.5*	*2.05*
1319	P47875	Cysteine and glycine-rich protein-1	21,455	8.9	58/56	6/44	51	−7.38	−6.49
1323	P47875	Cysteine and glycine-rich protein-1	21,455	8.9	91/56	7/40	54	13.77	13.41
416	Q5XI50	E3 ubiquitin–protein ligase MARCH7	76,932	7.64	53/51	9/44	16	*−2.86*	*−1.42*
709	P62630	Elongation factor-1α1	50,424	9.1	87/56	11/35	29	−2.01	−2.76
1244	O08719	Ena/VASP-like protein	42,183	8.74	59/51	6/43	20	*2.27*	*1.9*
305	Q99PF5	Far upstream element-binding protein-2	74,466	6.38	169/56	20/43	41	*−2.09*	*−1.21*
661	P07323	γ-Enolase	47,510	5.03	83/51	14/34	23	**−1.04**	**−1.65**
1251	Q9Z1B2	Glutathione S-transferase Mu 5	27,067	6.33	76/56	15/54	50	*−4.85*	*−1.82*
1255	P42930	Heat shock protein-β1	22,936	6.12	147/56	12/65	56	*−3.9*	*−1.11*
954	Q6RUG5	Islet cell autoantigen-1-like protein	49,298	5.23	54/51	9/53	31	−1.64	−1.36
1240	O35760	Isopentenyl diphosphate δ-isomerase-1	26,721	5.57	61/56	6/58	38	−1.8	−1.56
1237	Q63279	Keratin, type I cytoskeletal-19	44,609	5.21	51/51	10/73	25	*4.02*	*−1.15*
1219	Q6QLM7	Kinesin heavy chain isoform-5A	117,642	5.56	54/51	12/43	15	−2	−1.62
418	P56536	Kinesin heavy chain isoform-5C (fragment)	27,376	5.87	63/51	6/40	25	−2.7	−1.46
349	P48679	Lamin A	74,564	6.54	221/56	32/68	48	−2.04	−1.9
968	P04636	Malate dehydrogenase (mitochondrial)	36,117	8.93	128/56	15/55	51	−1.47	−1.52
1355	P13832	Myosin regulatory light chain RLC-A	19,940	4.67	102/56	13/52	62	2.18	2.21
1357	Q64122	Myosin regulatory light polypeptide-9	19,765	4.8	68/51	10/48	42	2.12	2.38
856	Q561S0	NADH dehydrogenase 1α subcomplex subunit-10	40,753	7.64	91/56	8/25	35	**−1.13**	**−1.77**
1276	Q63716	Peroxiredoxin-1	22,323	8.27	77/56	7/44	41	−1.84	−1.9
1213	P97562	Peroxisomal acyl-coenzyme A oxidase-2	77,548	7.64	53/51	10/41	17	*2.19*	*1.9*
1198	P25113	Phosphoglycerate mutase-1	28,928	6.67	72/51	8/28	40	−1.66	−5.13
1202	P25113	Phosphoglycerate mutase-1	28,928	6.67	169/56	22/59	60	1.41	1.63
1405	P62963	Profilin-1	15,119	8.46	94/56	11/44	75	*−3.01*	*1.43*
1242	P40112	Proteasome subunit β type-3	23,235	6.15	60/51	9/50	43	−3.09	−2.31
1300	P34067	Proteasome subunit β type-4	29,349	6.45	70/56	12/62	34	*6.23*	*5.32*
1321	P28075	Proteasome subunit β type-5	28,738	6.52	75/56	8/48	35	*15.04*	*13.2*
1301	Q6IML7	Rab and DnaJ domain-containing protein	31,329	8.72	54/51	6/30	26	−3.01	−3.17
781	P29315	Ribonuclease inhibitor	51,653	4.67	174/56	18/64	57	−1.56	−1.14
397	P48721	Stress-70 protein (mitochondrial)	74,097	5.97	103/56	21/79	33	*−2.12*	*−1.18*
1208	Q91Y78	Ubiquitin carboxyl-terminal hydrolase isozyme L3	26,278	5.01	124/56	13/43	63	*−1.64*	*−1.28*
782	P31000	Vimentin	53,757	5.06	249/56	32/59	64	**−1.06**	**1.82**

[a] Average ratio of differential expression ($p < 0.05$) between H_2O_2-treated and untreated cells (Ctrl) and PP1 + H_2O_2-treated and Ctrl cells calculated from triplicate gels. Italic type indicates proteins for which the changes between H_2O_2/Ctrl are significantly greater than the changes between PP1 + H_2O_2/Ctrl. Bold type indicates PP1-specific changes.

H_2O_2-treated and the untreated cells (Table 2). These data confirm that blocking Src kinase activity can partially, if not completely, rescue H_2O_2-induced protein expression changes that may be involved in H9C2 cell survival and/or adhesion. However, it must be noted that PP1-specific changes were also detected (Table 2, bold type), as were H_2O_2-mediated changes that seemed to be augmented by PP1 pretreatment.

Discussion

Myocardial damage induced by ischemia–reperfusion is largely due to the generation of ROS. If one can modulate the production of ROS by means of treating the tissue with antioxidants or blocking signaling-related ROS generation, then the ROS-induced effects of ischemia–reperfusion and myocardial dysfunction could be alleviated. Based on this concept, several studies have evaluated the effects of antioxidants on myocardial ischemia and reperfusion injury in animals and patients [43–47]. However, an incomplete understanding of the roles of ROS in myocardial ischemia and reperfusion injury together with the seemingly inconsistent results regarding the effects of antioxidants have discouraged their therapeutic application.

H_2O_2 is the most dominant form of the ROS and has been reported to play an important role in reversible protein phosphorylation. Accordingly, we first determined the optimal concentration of H_2O_2 to apply for redox studies in the rat heart cardiomyocyte cell line H9C2, a widely used model in ischemia and reperfusion studies that retains the characteristics of isolated primary myocytes [48–52]. Pilot experiments determined that treatment of H9C2 cells with 1 mM hydrogen peroxide for 20 min was sufficient to elicit a significant cellular response (activation of Akt, p38, and induction of tyrosine phosphorylation), while maintaining ~80% cell viability.

Protein tyrosine phosphatases are major targets of ROS and primary regulators of cellular tyrosine kinases. We therefore investigated ROS-induced tyrosine phosphorylation events in H9C2 cells and identified a subset of target proteins using an affinity-purification and LC–MS/MS strategy. More than 80% of the identified proteins are known to be involved in regulating the cytoskeleton and cell adhesion. Taking advantage of bioinformatic and biochemical tools, we found evidence that the Src kinase plays a central role in eliciting H_2O_2-induced tyrosine phosphorylation, which we linked directly to changes in the cytoskeleton and cell morphology, the loss of intercellular connections, cell detachment, and apoptosis. Importantly, we showed that blocking Src kinase activity could reverse

these effects. Our findings are similar to those observed in epithelial cells in which EGFR/Src were identified as the major kinases responsible for H_2O_2-induced phosphorylation of adhesion complexes, loss of adhesion, and apoptosis [53].

In a previous study, members of the Src family of tyrosine kinases were reported to be rapidly activated during ischemia–reperfusion injury [54], and Src kinase acts as a membrane growth factor receptor-associated molecule to switch crucial intracellular signaling pathways related to cell survival and death [55]. Our study confirms that Src kinase activation plays a key role in mediating myocardial injury during H_2O_2-induced ischemia–reperfusion and suggests that the inhibition of Src kinase activity might be an effective therapy for alleviating ROS-induced cell damage and death. Importantly, we also observed that H_2O_2 can activate the PI3K/Akt pathway via Src activation. Although PI3K/Akt pathway activation is normally known to promote cell survival, we proposed that the overactivation of the pathway in response to oxidative stress may have the reverse effect.

Src kinase family members have been implicated in regulating cell adhesion through the modulation of focal adhesion and cell junctional protein complexes. For example, Src kinase has been reported to phosphorylate and disrupt cadherin/catenin-mediated homotypic adhesion junctions [56]. The reorganization and disassembly of adhesion junctions in our system is likely to occur through the same mechanism, i.e., ROS-induced activation of Src leads to hyperphosphorylation and dissociation of catenin and M-cadherin and subsequent adherens junction disassembly and de-adhesion. The role of Src kinases in regulating tight junctions is less clear. However, our immunofluorescence data suggested that Src kinase may play a role in destabilizing tight junctions through proteins such as ZO-2. In support of this, a previous study showed that activated Src can phosphorylate junction plakoglobin at pTyr643, leading to its decreased interaction with E-cadherin and α-catenin [57]. In focal adhesions, the interplay of focal adhesion molecules and Src phosphorylation in coupling actin dynamics and motility signaling has been intensely studied; however, little is known about these processes in cardiomyocytes. Our data support the notion that Src plays a critical role in regulating focal adhesions in these cells and that oxidative stress mediates its effect on adhesion through activation of Src kinases. ROS have been shown to promote FAK, paxillin, and p130CAS tyrosine phosphorylation in endothelial cells [58], and similarly, we report that FAK1, FAK2, and p130CAS are hyperphosphorylated in ROS-treated cardiomyocytes, a situation that seems to favor de-adhesion. Gross reorganization of the actin cytoskeleton and changes in cell morphology were also observed in H9C2 cells in response to peroxide treatment, and various actin-binding/modulator proteins were identified in anti-phosphotyrosine immunoprecipitates. These proteins are also likely to be targets of ROS-induced Src kinase activation, resulting in the observed cytoskeletal reorganization.

The interplay between Src family kinases and RTKs is well established and it is known that PDGFR activity stimulates Src activity and vice versa [59]. In addition, redox regulation of PDGFR stimulation involving PKC, PI3K, and NADPH oxidase activity has been shown to contribute to full Src kinase activation, in turn promoting maximal tyrosine phosphorylation and activation of PDGFR [60]. In our study, we observed that blockade of Src kinase activity with PP1 could dramatically inhibit H_2O_2-induced tyrosine phosphorylation of PDGFR, suggesting a regulatory role for Src kinase on PDGFR activation under oxidative stress. In terms of a mechanism by which H_2O_2 activates the PDGFR and Src kinases, we propose that PTPs with PDGFR and/or Src as their substrate are targets of direct H_2O_2-mediated oxidative modification and inhibition. For PDGFR, LMW-PTP, PTP-PEST, SHP-2, PTP-1B, and T-cell PTP have all been reported to dephosphorylate the receptor [61,62]. In the case of Src, one previous study suggested a mechanism whereby PTP-BL/PTP-BAS can dephos-

phorylate pY416 of Src to inactivate it, and we speculate that this PTP may be inhibited by H_2O_2 [63].

Even though our experimental data showed PP1 to inhibit Src kinase and it has been widely used in kinase research, one needs to be careful in the interpretation of these data as PP1 shows some specificity toward other kinases, including p38, CSK, Bcr-Abl, and PDGFR [64,65]. This increases the complexity of studying Src kinase-dependent signaling events using this reagent and could explain some of our observations such as the inhibition of peroxide-induced p38 and PDGF-β receptor activation by PP1. Therefore, more specific inhibitors should be tested for their ability to block peroxide-induced tyrosine phosphorylation and cell detachment. Alternatively, small interfering RNAs targeting Src kinase expression could be in this system. Finally, this study has clinical implications because it identifies Src kinase as a potential therapeutic target in medical conditions in which oxidative stress is involved, such as ischemia–reperfusion injury of lung, heart, and kidney, among others, and in chronic lung disease, diabetes, Alzheimer disease, and atherosclerosis [66–70]. Thus, Src kinase inhibitors should be tested in animal models to validate their potential therapeutic application.

Acknowledgments

References

[1] Hunter, T. Protein kinases and phosphatases: the yin and yang of protein phosphorylation and signaling. *Cell* **80:**225–236; 1995.
[2] Pawson, T.; Nash, P. Assembly of cell regulatory systems through protein interaction domains. *Science* **300:**445–452; 2003.
[3] Krebs, E. G. The growth of research on protein phosphorylation. *Trends Biochem. Sci.* **19:**439; 1994.
[4] Cooper, J. A.; Sefton, B. M.; Hunter, T. Detection and quantification of phosphotyrosine in proteins. *Methods Enzymol.* **99:**387–402; 1983.
[5] Blume-Jensen, P.; Hunter, T. Oncogenic kinase signalling. *Nature* **411:**355–365; 2001.
[6] McLachlin, D. T.; Chait, B. T. Analysis of phosphorylated proteins and peptides by mass spectrometry. *Curr. Opin. Chem. Biol.* **5:**591–602; 2001.
[7] Sun, X.; Chiu, J. F.; He, Q. Y. Application of immobilized metal affinity chromatography in proteomics. *Expert Rev. Proteomics* **2:**649–657; 2005.
[8] Zhou, H.; Watts, J. D.; Aebersold, R. A systematic approach to the analysis of protein phosphorylation. *Nat. Biotechnol.* **19:**375–378; 2001.
[9] Schumacher, J. A.; Crockett, D. K.; Elenitoba-Johnson, K. S.; Lim, M. S. Evaluation of enrichment techniques for mass spectrometry: identification of tyrosine phosphoproteins in cancer cells. *J. Mol. Diagn.* **9:**169–177; 2007.
[10] Emadali, A.; Metrakos, P. P.; Kalantari, F.; Boutros, T.; Boismenu, D.; Chevet, E. Proteomic analysis of tyrosine phosphorylation during human liver transplantation. *Proteome Sci.* **5:**1; 2007.
[11] D'Autreaux, B.; Toledano, M. B. ROS as signalling molecules: mechanisms that generate specificity in ROS homeostasis. *Nat. Rev. Mol. Cell Biol.* **8:**813–824; 2007.
[12] Takano, H.; Zou, Y.; Hasegawa, H.; Akazawa, H.; Nagai, T.; Komuro, I. Oxidative stress-induced signal transduction pathways in cardiac myocytes: involvement of ROS in heart diseases. *Antioxid. Redox Signal.* **5:**789–794; 2003.
[13] Scandalios, J. G. The rise of ROS. *Trends Biochem. Sci.* **27:**483–486; 2002.
[14] Rhee, S. G.; Chang, T. S.; Bae, Y. S.; Lee, S. R.; Kang, S. W. Cellular regulation by hydrogen peroxide. *J. Am. Soc. Nephrol.* **14:**S211–S215; 2003.
[15] Barrett, W. C.; DeGnore, J. P.; Keng, Y. F.; Zhang, Z. Y.; Yim, M. B.; Chock, P. B. Roles of superoxide radical anion in signal transduction mediated by reversible regulation of protein-tyrosine phosphatase 1B. *J. Biol. Chem.* **274:**34543–34546; 1999.
[16] Finkel, T. Redox-dependent signal transduction. *FEBS Lett.* **476:**52–54; 2000.
[17] Kwon, J.; Lee, S. R.; Yang, K. S.; Ahn, Y.; Kim, Y. J.; Stadtman, E. R.; Rhee, S. G. Reversible oxidation and inactivation of the tumor suppressor PTEN in cells stimulated with peptide growth factors. *Proc. Natl Acad. Sci. U. S. A.* **101:**16419–16424; 2004.
[18] Ross, S. H.; Lindsay, Y.; Safrany, S. T.; Lorenzo, O.; Villa, F.; Toth, R.; Clague, M. J.; Downes, C. P.; Leslie, N. R. Differential redox regulation within the PTP superfamily. *Cell Signal.* **19:**1521–1530; 2007.
[19] Rhee, S. G.; Kang, S. W.; Jeong, W.; Chang, T. S.; Yang, K. S.; Woo, H. A. Intracellular messenger function of hydrogen peroxide and its regulation by peroxiredoxins. *Curr. Opin. Cell Biol.* **17:**183–189; 2005.

[20] Ferrari, R.; Ceconi, C.; Curello, S.; Cargnoni, A.; Pasini, E.; De Giuli, F.; Albertini, A. Role of oxygen free radicals in ischemic and reperfused myocardium. Am. J. Clin. Nutr. 53:215S–222S; 1991.

[21] Venardos, K. M.; Kaye, D. M. Myocardial ischemia–reperfusion injury, antioxidant enzyme systems, and selenium: a review. Curr. Med. Chem. 14:1539–1549; 2007.

[22] Zhao, Z. Q. Oxidative stress-elicited myocardial apoptosis during reperfusion. Curr. Opin. Pharmacol. 4:159–165; 2004.

[23] Saini, H. K.; Machackova, J.; Dhalla, N. S. Role of reactive oxygen species in ischemic preconditioning of subcellular organelles in the heart. Antioxid. Redox Signal. 6:393–404; 2004.

[24] Zima, A. V.; Blatter, L. A. Redox regulation of cardiac calcium channels and transporters. Cardiovasc. Res. 71:310–321; 2006.

[25] Saini, H. K.; Machackova, J.; Dhalla, N. S. Role of reactive oxygen species in ischemic preconditioning of subcellular organelles in the heart. Antioxid. Redox Signal. 6:393–404; 2004.

[26] Kwon, J. H.; Kim, J. B.; Lee, K. H.; Kang, S. M.; Chung, N.; Jang, Y.; Chung, J. H. Protective effect of heat shock protein 27 using protein transduction domain-mediated delivery on ischemia/reperfusion heart injury. Biochem. Biophys. Res. Commun. 363:399–404; 2007.

[27] Pchejetski, D.; Kunduzova, O.; Dayon, A.; Calise, D.; Seguelas, M. H.; Leducq, N.; Seif, I.; Parini, A.; Cuvillier, O. Oxidative stress-dependent sphingosine kinase-1 inhibition mediates monoamine oxidase A-associated cardiac cell apoptosis. Circ. Res. 100:41–49; 2007.

[28] Fiorillo, C.; Ponziani, V.; Giannini, L.; Cecchi, C.; Celli, A.; Nassi, N.; Lanzilao, L.; Caporale, R.; Nassi, P. Protective effects of the PARP-1 inhibitor PJ34 in hypoxic-reoxygenated cardiomyoblasts. Cell. Mol. Life Sci. 63:3061–3071; 2006.

[29] Zhang, Y. Q.; Herman, B. ARC protects rat cardiomyocytes against oxidative stress through inhibition of caspase-2 mediated mitochondrial pathway. J. Cell. Biochem. 99:575–588; 2006.

[30] Su, C. Y.; Chong, K. Y.; Owen, O. E.; Dillmann, W. H.; Chang, C.; Lai, C. C. Constitutive and inducible hsp70s are involved in oxidative resistance evoked by heat shock or ethanol. J. Mol. Cell Cardiol. 30:587–598; 1998.

[31] Han, H.; Long, H.; Wang, H.; Wang, J.; Zhang, Y.; Wang, Z. Progressive apoptotic cell death triggered by transient oxidative insult in H9c2 rat ventricular cells: a novel pattern of apoptosis and the mechanisms. Am. J. Physiol. Heart Circ. Physiol. 286:H2169–H2182; 2004.

[32] Neuhoff, V.; Arold, N.; Taube, D.; Ehrhardt, W. Improved staining of proteins in polyacrylamide gels including isoelectric focusing gels with clear background at nanogram sensitivity using Coomassie Brilliant Blue G-250 and R-250. Electrophoresis 9:255–262; 1988.

[33] Chan, H. L.; Gharbi, S.; Gaffney, P. R.; Cramer, R.; Waterfield, M. D.; Timms, J. F. Proteomic analysis of redox- and ErbB2-dependent changes in mammary luminal epithelial cells using cysteine- and lysine-labelling two-dimensional difference gel electrophoresis. Proteomics 5:2908–2926; 2005.

[34] Gharbi, S.; Gaffney, P.; Yang, A.; Zvelebil, M. J.; Cramer, R.; Waterfield, M. D.; Timms, J. F. Evaluation of two-dimensional differential gel electrophoresis for proteomic expression analysis of a model breast cancer cell system. Mol. Cell. Proteomics 1:91–98; 2002.

[35] Lai, T. C.; Chou, H. C.; Chen, Y. W.; Lee, T. R.; Chan, H. T.; Shen, H. H.; Lee, W. T.; Lin, S. T.; Lu, Y. C.; Wu, C. L.; Chan, H. L. Secretomic and proteomic analysis of potential breast cancer markers by two-dimensional differential gel electrophoresis. J. Proteome Res. 9:1302–1322; 2010.

[36] Inge, L. J.; Rajasekaran, S. A.; Wolle, D.; Barwe, S. P.; Ryazantsev, S.; Ewing, C. M.; Isaacs, W. B.; Rajasekaran, A. K. alpha-Catenin overrides Src-dependent activation of beta-catenin oncogenic signaling. Mol. Cancer Ther. 7:1386–1397; 2008.

[37] Karni, R.; Gus, Y.; Dor, Y.; Meyuhas, O.; Levitzki, A. Active Src elevates the expression of beta-catenin by enhancement of cap-dependent translation. Mol. Cell. Biol. 25:5031–5039; 2005.

[38] Martinez-Quiles, N.; Ho, H. Y.; Kirschner, M. W.; Ramesh, N.; Geha, R. S. Erk/Src phosphorylation of cortactin acts as a switch on–switch off mechanism that controls its ability to activate N-WASP. Mol. Cell. Biol. 24:5269–5280; 2004.

[39] Sun, C. K.; Man, K.; Ng, K. T.; Ho, J. W.; Lim, Z. X.; Cheng, Q.; Lo, C. M.; Poon, R. T.; Fan, S. T. Proline-rich tyrosine kinase 2 (Pyk2) promotes proliferation and invasiveness of hepatocellular carcinoma cells through c-Src/ERK activation. Carcinogenesis 29:2096–2105; 2008.

[40] Goldberg, G. S.; Alexander, D. B.; Pellicena, P.; Zhang, Z. Y.; Tsuda, H.; Miller, W. T. Src phosphorylates Cas on tyrosine 253 to promote migration of transformed cells. J. Biol. Chem. 278:46533–46540; 2003.

[41] Klinghoffer, R. A.; Sachsenmaier, C.; Cooper, J. A.; Soriano, P. Src family kinases are required for integrin but not PDGFR signal transduction. EMBO J. 18:2459–2471; 1999.

[42] Lee, K. M.; Villereal, M. L. Tyrosine phosphorylation and activation of pp 60c-src and pp125FAK in bradykinin-stimulated fibroblasts. Am. J. Physiol. 270: C1430–C1437; 1996.

[43] Hochhauser, E.; Kaminski, O.; Shalom, H.; Leshem, D.; Shneyvays, V.; Shainberg, A.; Vidne, B. A. Role of adenosine receptor activation in antioxidant enzyme regulation during ischemia–reperfusion in the isolated rat heart. Antioxid. Redox Signaling 6:335–344; 2004.

[44] Molyneux, C. A.; Glyn, M. C.; Ward, B. J. Oxidative stress and cardiac microvascular structure in ischemia and reperfusion: the protective effect of antioxidant vitamins. Microvasc. Res. 64:265–277; 2002.

[45] Barta, E.; Pechan, I.; Cornak, V.; Luknarova, O.; Rendekova, V.; Verchovodko, P. Protective effect of alpha-tocopherol and l-ascorbic acid against the ischemic–reperfusion injury in patients during open-heart surgery. Bratisl. Lek. Listy 92: 174–183; 1991.

[46] Westhuyzen, J.; Cochrane, A. D.; Tesar, P. J.; Mau, T.; Cross, D. B.; Frenneaux, M. P.; Khafagi, F. A.; Fleming, S. J. Effect of preoperative supplementation with alpha-tocopherol and ascorbic acid on myocardial injury in patients undergoing cardiac operations. J. Thorac. Cardiovasc. Surg. 113:942–948; 1997.

[47] Demirag, K.; Askar, F. Z.; Uyar, M.; Cevik, A.; Ozmen, D.; Mutaf, I.; Bayindir, O. The protective effects of high dose ascorbic acid and diltiazem on myocardial ischaemia–reperfusion injury. Middle East J. Anesthesiol. 16:67–79; 2001.

[48] Kwon, J. H.; Kim, J. B.; Lee, K. H.; Kang, S. M.; Chung, N.; Jang, Y.; Chung, J. H. Protective effect of heat shock protein 27 using protein transduction domain-mediated delivery on ischemia/reperfusion heart injury. Biochem. Biophys. Res. Commun. 363:399–404; 2007.

[49] Pchejetski, D.; Kunduzova, O.; Dayon, A.; Calise, D.; Seguelas, M. H.; Leducq, N.; Seif, I.; Parini, A.; Cuvillier, O. Oxidative stress-dependent sphingosine kinase-1 inhibition mediates monoamine oxidase A-associated cardiac cell apoptosis. Circ. Res. 100:41–49; 2007.

[50] Fiorillo, C.; Ponziani, V.; Giannini, L.; Cecchi, C.; Celli, A.; Nassi, N.; Lanzilao, L.; Caporale, R.; Nassi, P. Protective effects of the PARP-1 inhibitor PJ34 in hypoxic-reoxygenated cardiomyoblasts. Cell. Mol. Life Sci. 63:3061–3071; 2006.

[51] Zhang, Y. Q.; Herman, B. ARC protects rat cardiomyocytes against oxidative stress through inhibition of caspase-2 mediated mitochondrial pathway. J. Cell. Biochem. 99:575–588; 2006.

[52] Su, C. Y.; Chong, K. Y.; Owen, O. E.; Dillmann, W. H.; Chang, C.; Lai, C. C. Constitutive and inducible hsp70s are involved in oxidative resistance evoked by heat shock or ethanol. J. Mol. Cell. Cardiol. 30:587–598; 1998.

[53] Chan, H. L.; Chou, H. C.; Duran, M.; Gruenewald, J.; Waterfield, M. D.; Ridley, A.; Timms, J. F. Major role of EGFR and SRC kinases in promoting oxidative stress-dependent loss of adhesion and apoptosis in epithelial cells. J. Biol. Chem. 285: 4307–4318; 2009.

[54] Takeishi, Y.; Abe, J.; Lee, J. D.; Kawakatsu, H.; Walsh, R. A.; Berk, B. C. Differential regulation of p90 ribosomal S6 kinase and big mitogen-activated protein kinase 1 by ischemia/reperfusion and oxidative stress in perfused guinea pig hearts. Circ. Res. 85:1164–1172; 1999.

[55] Johnson, D.; Agochiya, M.; Samejima, K.; Earnshaw, W.; Frame, M.; Wyke, J. Regulation of both apoptosis and cell survival by the v-Src oncoprotein. Cell Death Differ. 7:685–696; 2000.

[56] Irby, R. B.; Yeatman, T. J. Increased Src activity disrupts cadherin/catenin-mediated homotypic adhesion in human colon cancer and transformed rodent cells. Cancer Res. 62:2669–2674; 2002.

[57] Miravet, S.; Piedra, J.; Castano, J.; Raurell, I.; Franci, C.; Dunach, M.; Garcia, D. H. Tyrosine phosphorylation of plakoglobin causes contrary effects on its association with desmosomes and adherens junction components and modulates beta-catenin-mediated transcription. Mol. Cell. Biol. 23:7391–7402; 2003.

[58] Gozin, A.; Franzini, E.; Andrieu, V.; Da Costa, L.; Rollet-Labelle, E.; Pasquier, C. Reactive oxygen species activate focal adhesion kinase, paxillin and p130cas tyrosine phosphorylation in endothelial cells. Free Radic. Biol. Med. 25:1021–1032; 1998.

[59] Bromann, P. A.; Korkaya, H.; Courtneidge, S. A. The interplay between Src family kinases and receptor tyrosine kinases. Oncogene 23:7957–7968; 2004.

[60] Catarzi, S.; Biagioni, C.; Giannoni, E.; Favilli, F.; Marcucci, T.; Iantomasi, T.; Vincenzini, M. T. Redox regulation of platelet-derived-growth-factor-receptor: role of NADPH-oxidase and c-Src tyrosine kinase. Biochim. Biophys. Acta 1745: 166–175; 2005.

[61] Markova, B.; Herrlich, P.; Ronnstrand, L.; Bohmer, F. D. Identification of protein tyrosine phosphatases associating with the PDGF receptor. Biochemistry 42: 2691–2699; 2003.

[62] Chiarugi, P.; Cirri, P.; Taddei, M. L.; Giannoni, E.; Fiaschi, T.; Buricchi, F.; Camici, G.; Raugei, G.; Ramponi, G. Insight into the role of low molecular weight phosphotyrosine phosphatase (LMW-PTP) on platelet-derived growth factor receptor (PDGF-r) signaling: LMW-PTP controls PDGF-r kinase activity through TYR-857 dephosphorylation. J. Biol. Chem. 277:37331–37338; 2002.

[63] Palmer, A.; Zimmer, M.; Erdmann, K. S.; Eulenburg, V.; Porthin, A.; Heumann, R.; Deutsch, U.; Klein, R. EphrinB phosphorylation and reverse signaling: regulation by Src kinases and PTP-BL phosphatase. Mol. Cell 9:725–737; 2002.

[64] Tatton, L.; Morley, G. M.; Chopra, R.; Khwaja, A. The Src-selective kinase inhibitor PP1 also inhibits Kit and Bcr-Abl tyrosine kinases. J. Biol. Chem. 278:4847–4853; 2003.

[65] Bain, J.; Plater, L.; Elliott, M.; Shpiro, N.; Hastie, C. J.; McLauchlan, H.; Klevernic, I.; Arthur, J. S.; Alessi, D. R.; Cohen, P. The selectivity of protein kinase inhibitors: a further update. Biochem. J. 408:297–315; 2007.

[66] Lamendola, P.; Di Monaco, A.; Barone, L.; Pisanello, C.; Lanza, G. A.; Crea, F. Mechanisms of myocardial cell protection from ischemia/reperfusion injury and potential clinical implications. G. Ital. Cardiol. (Rome) 10:28–36; 2009.

[67] Kosieradzki, M.; Rowinski, W. Ischemia/reperfusion injury in kidney transplantation: mechanisms and prevention. Transplant. Proc. 40:3279–3288; 2008.

[68] Ovechkin, A. V.; Lominadze, D.; Sedoris, K. C.; Robinson, T. W.; Tyagi, S. C.; Roberts, A. M. Lung ischemia–reperfusion injury: implications of oxidative stress and platelet–arteriolar wall interactions. Arch. Physiol. Biochem. 113:1–12; 2007.

[69] Bonomini, F.; Tengattini, S.; Fabiano, A.; Bianchi, R.; Rezzani, R. Atherosclerosis and oxidative stress. Histol. Histopathol. 23:381–390; 2008.

[70] Spector, A. Oxidative stress and disease. J. Ocul. Pharmacol. Ther. 16:193–201; 2000.